THE JOURNAL OF PHYSICAL CHEMISTRY C

Article

pubs.acs.org/JPCC

Single-Molecule Level Insight into Nanoscale Environment-Dependent Photophysics in Blends

Rebecca Grollman,[†] Nicole Quist,[†] Alexander Robertson,[†] Jeremy Rath,[†] Balaji Purushothaman,[‡] Michael M. Haley,[§] John E. Anthony,[‡] and Oksana Ostroverkhova*[,†]

[†]Department of Physics, Oregon State University, Corvallis, Oregon 97331, United States

[‡]Department of Chemistry, University of Kentucky, Lexington, Kentucky 40506, United States

[§]Department of Chemistry & Biochemistry and the Materials Science Institute, University of Oregon, Eugene, Oregon 97403, United States

Supporting Information

ABSTRACT: Organic semiconductors have attracted considerable attention due to their applications in low-cost (opto)electronic devices. Many successful organic materials utilize blends of several types of molecules that contribute different functions (e.g., serving as donors and acceptors in solar cells). In blends, the local environment, which is inherently heterogeneous, strongly influences the (opto)electronic performance and photostability. We use functionalized fluorinated pentacene (F8 TCHS-Pn) molecules as single-molecule probes of the nanoscale environment in blends containing donor and acceptor molecules incorporated into a polymer (PMMA) matrix. Single F8 TCHS-Pn donor (D) molecules were imaged in PMMA in the presence of functionalized indenofluorene (TIPS-IF) or PCBM acceptor (A) molecules using wide-field fluorescence microscopy at various concentrations. Long-lived dark states attributed to a reversible formation of an endoperoxide (TCHS-EPO) were observed, and the EPO formation and reversal processes, which evolved upon acceptor addition, were quantified. Our study provides a nanoscale-level insight into how the presence of acceptor molecules alters the photophysics of the donor molecules dispersed in the polymer. Kinetics of the F8 TCHS-Pn photo-oxidation reaction and its reversal in such blends are determined by a fine balance of the acceptor-modified morphology (which in our case speeds up the photo-oxidation and slows down its reversal) and singlet oxygen quenching by acceptors (which prevents repeated photo-oxidation/reversal events).

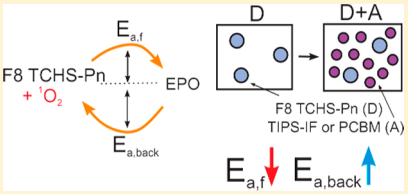

INTRODUCTION

Organic semiconductors have attracted attention due to their applications in low-cost, solution processable, and lightweight (opto)electronic devices; applications ranging from thin-film transistors (TFTs) to solar cells and photorefractive displays have been demonstrated, many of which have already been commercialized.[1] Regardless of the application, organic materials have several pertinent issues that need resolving. These include dependence of the (opto)electronic properties on nanoscale morphology (which is difficult to assess and to control) and low stability with respect to photo-oxidation, both of which are a subject of the present study.

Many successful organic (opto)electronic materials utilize blends of two or more types of molecules serving different functions. Some of the best performing TFTs utilize mixtures of small molecules (that provide high charge carrier mobility) with amorphous polymer (which provides enhanced processability), which have been shown to reduce trap densities and boost charge carrier mobilities as compared to pristine small-molecule films.[2] In solar cells and photorefractive materials, blends of polymers and small molecules (e.g., acting as the donor and acceptor, respectively) promote charge photogeneration. In any application, charge generation and/or transport considerably depend on the microstructure and morphology of the blend.[3,4] However, quantitative assessment of the nanoscale-level morphology in blends and, for example, how it affects the photophysics is not straightforward, so that even the highest-resolution methods such as scanning probe microscopies[5] do not provide the molecular-level relationship between the particular features of the molecular arrangements in the blend and resulting dynamics of photoinduced interactions.

Single-molecule fluorescence spectroscopy (SMFS) has elucidated various aspects of photophysics in molecules relevant for organic electronics.[1,6] In these experiments, most typical systems under study are ultralow concentrations of fluorescent molecules of interest incorporated into non-fluorescent amorphous polymer matrices (such as poly(methyl methacrylate) (PMMA) or poly(styrene) (PS)), and analysis of their fluorescence time trajectories may provide unique insights. Examples of these include nanoscale observations of photo-excited charge carrier diffusion,[7] chain folding-related fluorescence quenching,[8] exciton localization/delocalization char-

Received: April 20, 2017
Revised: May 17, 2017
Published: May 18, 2017

DOI: 10.1021/acs.jpcc.7b03729
J. Phys. Chem. C 2017, 121, 12483−12494

acteristics,[9,10] and elucidation of mechanisms and products of the photodegradation.[11−14]

We recently reported on photophysical properties of a variety of functionalized pentacene (Pn) and anthradithiophene derivatives with high fluorescence quantum yields (QYs) and photostability, which makes them suitable for room-temperature SMFS studies in air.[15] These molecules have been widely utilized in organic electronic devices,[2,16−19] and therefore, issues pertaining to the photophysics and stability affected by the nanoscale morphology are important for further utility of these molecules in applications and molecular design of improved structures.[20−23] One such derivative, a stable fluorinated Pn functionalized with tricyclohexylsilylethynyl (TCHS) side groups, F8 TCHS-Pn, is utilized as a single-molecule reporter, incorporated in PMMA, in the present study. As discussed above, an important consideration for organic semiconductor blends is how the nanoscale morphology evolves as molecules of other types (e.g., acceptors) are added to the blend. To mimic such evolution (e.g., occurring in the process of bulk heterojunction (BHJ) formation or in BHJs with different compositions), we gradually add acceptor molecules, either a functionalized indenofluorene (IF) derivative[17,24,25] or a "universal acceptor" PCBM,[26] to the F8 TCHS-Pn:PMMA samples and monitor changes in the photophysics of the F8 TCHS-Pn molecules. In particular, we use SMFS to establish (i) how the nanoscale environment in a polymer evolves upon addition of acceptor molecules and (ii) how the presence of acceptors influences interactions of the donor with oxygen and resulting photodegradation and its reversal.

EXPERIMENTAL SECTION

Sample Preparation. The following types of films were prepared for single-molecule imaging: (i) plain F8 TCHS-Pn (donor-only samples) at varying donor concentrations, (ii) F8 TCHS-Pn at a fixed concentration, but with varying concentrations of added acceptor molecules, either PCBM ([C60]PCBM obtained from Nano-C) or TIPS-IF, and (iii) TIPS-IF at a fixed concentration, with varied concentrations of F8 TCHS-Pn donor molecules. Molecular structures are shown in Figure 1(a). Both donor and acceptor molecules served as guest molecules in a PMMA (75 000 m.w., Polysciences, Inc.) host. Samples were prepared in a 1 wt % solution of PMMA in toluene with a fluorophore (F8 TCHS-Pn) concentration of a multiple of 3.4×10^{-10} M, which served as our baseline concentration (1×). Acceptor (TIPS-IF or PCBM) molecules were added to achieve varied average acceptor−acceptor spacings based on the molar fraction of the acceptor and PMMA as detailed in our previous studies[27,28] and in the Supporting Information. Most data were obtained in donor-only samples at 1× and 2× donor concentrations and in donor−acceptor samples at 1× donor concentrations when the average acceptor−acceptor separation was in the range of 6−20 nm and at 6×−100× at the average acceptor−acceptor separation of 5 nm. Other concentrations were also used for intermolecular distance calibration purposes, as described in the Supporting Information. Slide preparation and cleanliness controls followed the procedures of ref 15 and are described in the Supporting Information. Cleanliness of all constituents (coverslip, toluene, pristine PMMA host, and acceptor-only samples) was ensured each time before proceeding with preparing samples of interest by imaging them under the same experimental conditions as the donor-only or donor−acceptor samples. All films were spun at 3000 rpm for 50 s from

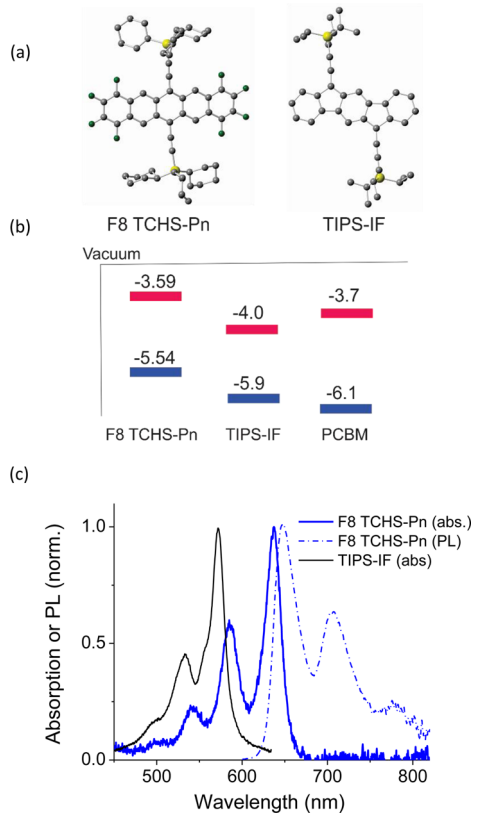

Figure 1. (a) Molecular structures of F8 TCHS-Pn and TIPS-IF and (b) HOMO/LUMO energy levels of the donor (F8 TCHS-Pn) and acceptor (TIPS-IF and PCBM) molecules under study. (c) Absorption spectra of F8 TCHS-Pn and TIPS-IF molecules and PL spectrum of F8 TCHS-Pn molecules in toluene.

60 μL of solution and had a thickness of 19 ± 2 nm as confirmed by AFM.

Single-Molecule Imaging and Analysis. Single-molecule fluorescence imaging of F8 TCHS-Pn molecules was performed under circularly polarized 633 nm wide-field illumination using an Olympus IX-71 inverted microscope with a 100× UPlanSApo (NA 1.4) oil objective and an Andor iXon EMCCD (DU-897) detector using integration time of 100 ms as described in our previous work[15] and in the Supporting Information. The excitation power was about 70 W/cm^2, and the typical duration of the video was 100 s. On selected samples, up to 6 consecutive videos were taken from the same sample area (Figure S10).

Potential individual fluorophores were detected and their fluorescence time trajectories obtained, using custom MATLAB scripts. The time traces were selected for further analysis if the trace exhibited a two-level behavior with a digital "on"−"off"/"off"−"on" switching, with a threshold of three standard deviations above the average "off" count level. To ensure that the threshold choice did not affect the data processing due to noise, a custom MATLAB script was written to select traces that had events lasting less than 20 frames (each frame is 0.116 s) for further examination, and if the counts were only slightly below (above) the threshold for the "on" ("off") levels, then their durations were combined with those of the adjacent "on" ("off") events. From each type of the sample, fluorescence trajectories from ∼150−350 fluorophores were analyzed (Tables S1 and S2) depending on the sample and the type of

DOI: 10.1021/acs.jpcc.7b03729
J. Phys. Chem. C 2017, 121, 12483−12494

analysis. The cumulative distribution function (CDF) $S(t)$ was calculated directly from collected "on" or "off" times t_i using[29]

$$S(t) = \frac{1}{N}\sum_i t_i \le t$$

where N is the total number of "on" ("off") events and t is a unique time in the set of collected "on" ("off") times. The complementary CDF (CCDF) is $F(t) = 1 - S(t)$. The last "off" ("on") time durations in the "nonblinker" ("blinker") "on"−"off" (e.g., "on"−"off"−"on") time traces were discarded from the analysis. The CCDFs for the "on" (for "blinkers" and "nonblinkers") and "off" (for "blinkers") times were fit to the single-exponential, power-law, Weibull, and log-normal functions using the maximum likelihood estimation (MLE) and Kolmogorov−Smirnov (KS) test.[29] Statistical p-tests were performed to assess the relevance of each function to the description of each data set (Table S2). Details of this analysis can be found in the Supporting Information.

To assess correlations between the "on" time and the preceding "off" time durations, we selected "blinker" time trajectories with well-defined "on" periods (i.e., those not limited by the duration of the video) following the "off" periods. In such trajectories, the "off" time duration was paired with the immediately following "on" time duration. In the figure showing the correlation between the "on" and the preceding "off" time durations, each data point for the "on" time duration corresponds to an average over an 8 s window of the corresponding "off" time duration. Donor-only traces include data from 84 "blinker" fluorophore traces from two donor-only samples, while the donor−acceptor traces include data from 123 "blinker" fluorophore traces from two donor−acceptor samples with a 5 nm-spaced TIPS-IF acceptor.

RESULTS

Donor−Acceptor Systems under Study. For our studies, we selected a functionalized fluorinated Pn derivative, F8 TCHS-Pn, as the donor and a functionalized IF derivative, TIPS-IF, and PCBM as acceptors (Figure 1). Both donor and acceptor molecules were incorporated in PMMA. The choice of these molecules was inspired by our previous work with these materials in organic donor−acceptor BHJ devices[17,19] and particular considerations discussed next.

The F8 R-Pn derivatives incorporated in PMMA at ultralow concentrations have been studied at the single-molecule level using SMFS and shown to exhibit high fluorescence QY (~0.7−0.8, depending on the side group R) and considerably higher photostability than the nonfluorinated functionalized Pn derivatives (such as TIPS-Pn).[15] Of all the studied F8 R-Pn derivatives incorporated in PMMA, the derivative functionalized with the bulkiest TCHS side groups, F8 TCHS-Pn, demonstrated the highest photostability in air ($\Phi_B \sim 10^{-6}$, which is the probability of photobleaching upon absorption of a photon), indicative of a protective role of these groups with respect to reactions with oxygen. However, how the degree of such protection depends on the local nanoenvironment has not yet been elucidated and is one of the insights revealed in the present study.

The IF and PCBM derivatives have been used as acceptors and/or electron transporting materials in a variety of organic (opto)electronic devices due to their low LUMO energies (Figure 1(b)).[1,17,30−33] Important for our present studies is that both TIPS-IF and PCBM feature very low fluorescence QYs (for example, TIPS-IF has a short, 9.7 ps excited-state lifetime due to efficient nonradiative decay via conical intersection[34]). This enabled us to incorporate relatively high concentrations of these molecules into PMMA without considerably raising the fluorescence background at 633 nm excitation used in our experiments that efficiently excites F8 TCHS-Pn molecules (Figure 1(c)). In particular, we were able to monitor changes in the photophysics of single F8 TCHS-Pn fluorophores due to changes in the nanoenvironment induced by an addition of acceptor molecules at concentrations such that the average acceptor−acceptor separation was varied between 5 and 20 nm (Figure 2(a)) and compare observations in various donor−acceptor samples to those in donor-only samples. The TIPS-IF acceptor was the main acceptor choice in our experiments. Detailed studies of samples with high PCBM concentrations were not carried out to minimize effects of Pn−fullerene reactions during the sample preparation[35] on the data; however, experiments with low PCBM concentrations and selected experiments at high concentrations revealed similar trends to those in samples with TIPS-IF acceptors.

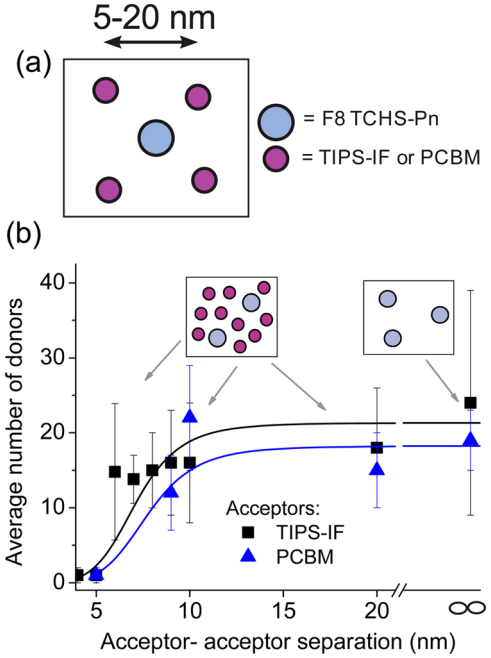

Figure 2. (a) Schematics of the experimental configurations under study: ultralow concentrations of the F8 TCHS-Pn donor and either PCBM or TIPS-IF acceptor at concentrations that yield average acceptor−acceptor separations varying between 5 and 20 nm, all dispersed in PMMA. Donor-only (in PMMA) samples were also studied. (b) Average number of F8 TCHS-Pn molecules in the field of view (area with a ~ 40 μm diameter), at a fixed donor concentration (3.4×10^{-10} M, or 1×), depending on the average acceptor−acceptor separation, where the infinite separation corresponds to donor-only samples. At average acceptor−acceptor separations of below ~$2R_0$ (where R_0 is a FRET radius), no F8 TCHS-Pn molecules are detected in samples with 1× donor concentrations due to efficient FRET, and the donor concentration must be increased to increase the probability of F8 TCHS-Pn donor to be located at a distance further than R_0 from the nearest acceptor. Error bars reflect area-to-area variation in the number of observed fluorophores in each sample. Lines are fits to the distance-dependent FRET efficiency.

Details on sample preparation and on conversion between concentrations of molecules used and resulting average

DOI: 10.1021/acs.jpcc.7b03729
J. Phys. Chem. C 2017, 121, 12483−12494

acceptor−acceptor separation can be found in the Experimental Section and in the Supporting Information. An additional calibration of intermolecular distances is enabled by the Förster resonance energy transfer (FRET) between F8 TCHS-Pn donor and TIPS-IF or PCBM acceptors (Figures 2(b) and S1−S4) occurring at donor−acceptor distances lower than the FRET radius (R_0) of 2.7 nm (3.4 nm) for TIPS-IF (PCBM). Under our experimental conditions for single-molecule imaging, F8 TCHS-Pn donor molecules that were within the FRET radius of the nearest acceptor molecule appeared dark, thus excluding this population from our studies. This effect is illustrated in Figures 2(b) and S3, which show a dramatic decrease in the number of detected fluorophores as the average acceptor−acceptor separation decreases below the $2R_0$ value. Therefore, at the 5 nm average acceptor−acceptor separation, higher donor concentrations (as compared to those in all other donor−acceptor samples) were used to increase the probability of obtaining the donor−acceptor spacing higher than R_0, as discussed in detail in the Supporting Information. In this case, FRET also served as a super-resolution tool enabling experiments at donor concentrations of up to 2 orders of magnitude higher than that used in our donor-only samples, ensuring that only one donor molecule is emissive within the diffraction limited image (Figures S1−S3).

The considerations above ensured that single donor molecules under study were spaced at least ∼3−3.5 nm away from the nearest acceptor molecule. Therefore, they do not directly participate in energy or charge transfer interactions with the acceptor but rather serve as sensors for acceptor-induced changes in local nanoenvironment that are important for their photophysics.

Effect of Acceptor Addition on Fluorescence Time Trajectories. The total number of detected photons ($N_{tot,det}$) was determined for each sample by integrating individual time traces (Figure 3(a)) to construct histograms (Figure 3(b)) of the number of detected photons N_{det}. The histograms showed satisfactory fits to a single-exponential function $\exp[-N_{det}/N_{tot,det}]$,[15,36,37] which has previously served as an indicator of photobleaching mechanism not involving two-photon processes such as excited-state absorption.[37] Involvement of higher excited states is not expected due to a low excitation intensity and the wavelength which does not invoke the $T_1 - T_n$ transitions[38] used in our experiments.[12,13,39] As shown in the inset of Figure 3(b), the total number of detected photons $N_{tot,det}$ decreased at the average acceptor−acceptor separation of below 9 nm.

Another pronounced effect of acceptor addition was a consistent increase in blinking (Figure 4). Here we consider the molecule to be "blinking" when its fluorescence trajectory exhibits at least one "off"−"on" transition during our observation time of 100 s, whereas molecules with only one "on"−"off" transition are "nonblinking" (Figure 3(a)). While only ∼10−14% of F8 TCHS-Pn molecules are "blinkers" in donor-only samples, this number increases to over ∼50% in donor−acceptor samples at average acceptor−acceptor separation of less than 8 nm.

These observations are indicative of an acceptor-mediated change in the immediate environment of F8 TCHS-Pn single-molecule reporters that affects their photophysics, prompting detailed evaluation of kinetics of the transitions the molecule undergoes.

Evolution of Average "On" and "Off" Time Durations. To gain insight into the underlying processes behind

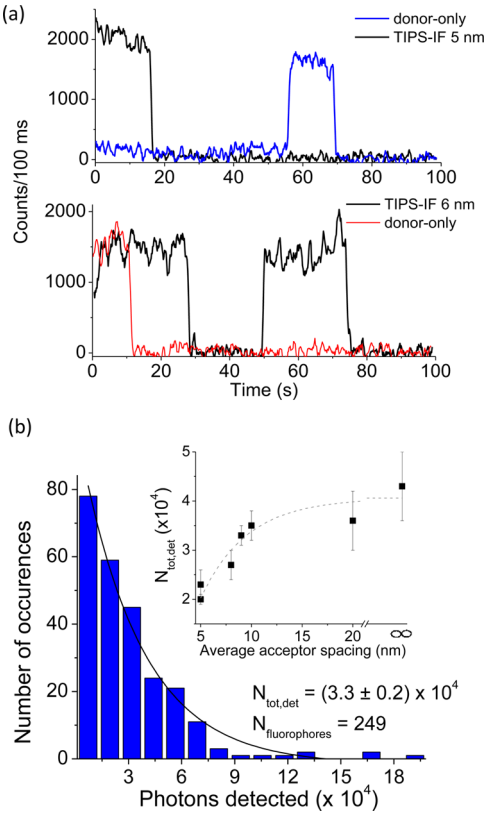

Figure 3. (a) Examples of "nonblinker" and "blinker" F8 TCHS-Pn fluorescence time trajectories obtained in donor-only and donor−acceptor samples with the average acceptor−acceptor separation indicated. (b) Example of a histogram obtained from an ensemble of 249 fluorophores in a donor−acceptor sample with 9 nm-spaced TIPS-IF acceptors and of a single-exponential ($\exp(-N_{det}/N_{tot,det})$) fit from which the total number of detected photons $N_{tot,det}$ was calculated. Inset shows a change in $N_{tot,det}$ as TIPS-IF acceptors are added. Line provides a guide for the eye.

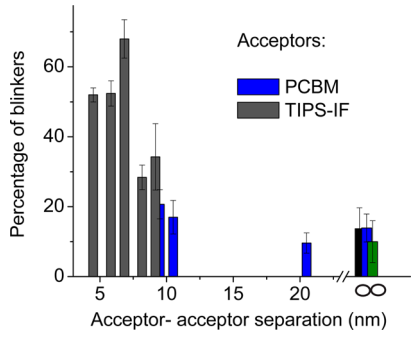

Figure 4. Percentage of "blinking" molecules (defined as those exhibiting at least one "off"−"on" event over the 100 s duration of experiment) depending on the average acceptor−acceptor separation. Error bars correspond to the area-to-area variation in each sample. Data from three different donor-only samples (infinite acceptor−acceptor separation) are also included.

observations of Figures 3(b) and 4, we separately analyzed the fluorescence time trajectories for "nonblinkers" and "blinkers". Because of our long integration time of 100 ms, microsecond time-scale blinking (e.g., due to the intersystem crossing (ISC)) is not detected (so that the molecule appears to be "on" even after the ISC from S_1 to T_1 occurred, provided it is then followed by the T_1−S_0 relaxation, S_0−S_1 re-excitation,

DOI: 10.1021/acs.jpcc.7b03729
J. Phys. Chem. C 2017, 121, 12483−12494

and emission).[40] Thus, all "blinking" events studied in our experiments are related to longer time-scale processes, with "on" and "off" time durations of at least 3 s and ~20−40 s on average, exemplified by the time traces shown in Figure 3(a). Processes involving long-lived dark states (characterized by long "off" times) have been previously attributed to charge transfer reactions, in which case the dark state is a charge-separated state (so the fluorescent parent molecule temporarily becomes a nonfluorescent ion), or to photo-oxidation reactions (so that the fluorescent parent molecule reacts with oxygen to create a dark intermediate followed by photo-oxidation products with different emission properties).[11,13,40] These scenarios as possible mechanisms behind our observations will be examined in the "Discussion".

From the observed "on" (for "blinkers" and "nonblinkers") and "off" (for "blinkers") time durations, the complementary cumulative distribution functions (CCDFs) were calculated directly from the experimental data[40,29] as described in the Experimental Section. Since most of the "blinking" molecules exhibited only one "blinking" event over our observation time, statistical analysis of single-molecule blinking events was not possible; thus, the data were compiled for ensembles of ~150−350 fluorophores, depending on the acceptor concentration (Tables S1 and S2). Examples of CCDFs obtained from such ensembles for "on" and "off" time intervals are shown in Figure 5, exhibiting trends toward shorter "on" and longer "off" time durations, on average, upon acceptor addition.

Next, the statistical p-tests were employed to identify the most probable distribution which describes the CCDF data, with the distributions tested including power-law, log-normal, Weibull, and single-exponential.[40,29,41] In most samples, the CCDFs for the "on" time durations (t_{on}) in "nonblinkers" were best described by the Weibull function CCDF = $\exp(-(t_{on}/\beta)^A)$, where A and β are fit parameters (Tables S2 and S3). For example, p = 0.93 and 0.48 were obtained for the "on" time CCDFs in a donor-only and in a donor−acceptor with 5 nm spaced acceptor samples, respectively, in Figure 5(a), with all other functions tested yielding $p \leq 0.03$ (Table S2). The average "on" times $\langle\tau\rangle_{on}$ calculated from the Weibull fit parameters using $\langle\tau\rangle_{on} = \beta\Gamma(1 + 1/A)$ (where Γ is the Gamma function) depending on the average acceptor−acceptor spacing are shown in Figure 6(a). A decrease is observed from (32 ± 1) s in donor-only samples to (14 ± 1) s in donor−acceptor samples at average acceptor−acceptor separation of 5 nm. The dominant factor in this behavior was the Weibull scaling parameter β which decreased upon acceptor addition, while the parameter A did not show any strong trends, yielding values between 1.3 and 1.6, depending on the sample (Table S3). In "blinkers", values of $\langle\tau\rangle_{on}$ were similar to those in "nonblinkers" in most samples (Figures 6(a) and S5), although the fit parameters A and β incorporated into the average time $\langle\tau\rangle_{on}$ for "blinkers" were slightly different than those for the "non-blinkers" (Table S3), which will be addressed later. Just as in "nonblinkers", the $\langle\tau\rangle_{on}$ in "blinkers" decreased upon acceptor addition (Figure 6(a)).

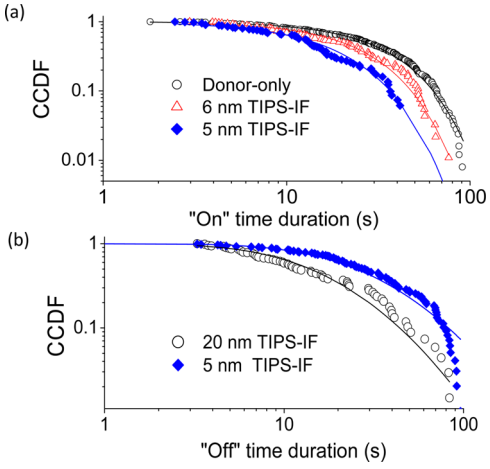

Figure 5. Complementary cumulative distribution functions (CCDFs) for (a) the "nonblinkers" "on" and (b) "blinkers" "off" time durations complied from ~90−170 fluorescence time trajectories, depending on the sample. The CCDF value at a given "on" or "off" time duration represents the probability of an "on" or "off" event to have the duration longer than the selected time. Fits to the data with functions that yielded highest p-values are also shown. The "on" CCDFs were predominantly Weibull-distributed (e.g., with a p-value of 0.93 for the donor-only sample shown), and Weibull fits ($\exp[-(t/\beta)^A]$) to the data are included. The "off" CCDFs exhibited either log-normal or Weibull behavior in donor-only samples and in donor−acceptor samples with acceptor−acceptor spacing of 20 nm, depending on the sample. Donor−acceptor samples with higher acceptor concentration showed predominantly Weibull distribution (e.g., p = 0.41 for the Weibull distribution in the donor−acceptor sample with 5 nm spaced TIPS-IF acceptor).

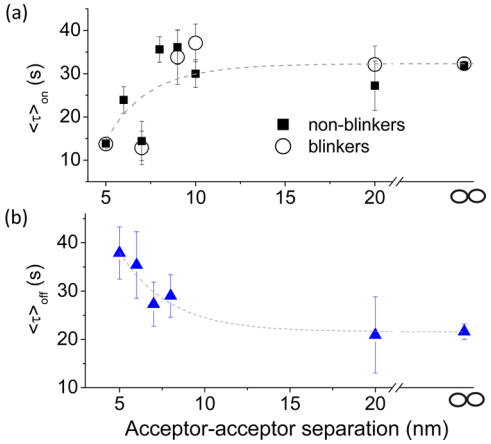

Figure 6. Average "on" (both for "nonblinkers" and "blinkers") (a) and "off" ("blinkers"-only) (b) time durations calculated from fit parameters (e.g., $\langle\tau\rangle = \beta\Gamma(1 + 1/A)$, where Γ is the Gamma function, and $\langle\tau\rangle = \exp[\mu + \sigma^2/2]$ in the case of Weibull and log-normal fits, respectively, where A, β, μ, and σ are fit parameters) depending on the average acceptor−acceptor separation. Lines provide a guide for the eye.

The p-tests for the "off" time (t_{off}) CCDFs also indicated preference for the Weibull distribution (so that CCDF = $\exp(-(t_{off}/\beta)^A)$, with the exception of some samples that favored the log-normal distribution (CCDF = $1 - (1/2)\mathrm{erfc}(-(\ln(t_{off}) - \mu)/(\sigma\sqrt{2}))$, where erfc is the complementary error function and μ and σ are fit parameters) (Tables S2 and S3).[29] The average "off" times calculated from the fit parameters are shown in Figure 6(b), exhibiting an increase in the average "off" time duration from 22 s in donor-only samples (Figure S5) to 38 s in donor−acceptor samples with the average acceptor−acceptor spacing of 5 nm. Similar to the "on" times, this trend mostly reflects an increase in the Weibull scaling parameter β upon acceptor addition; however, the Weibull parameter A also changes, increasing from 1.1 in

DOI: 10.1021/acs.jpcc.7b03729
J. Phys. Chem. C 2017, 121, 12483−12494

donor-only samples to 1.5 in donor−acceptor samples with 5 nm spaced acceptors.

The Weibull distribution function has been widely used in the analysis of fatigue behavior of materials and mechanical strength of complex materials,[42] as well as in descriptions of chemical reactions with distributed activation energies.[43,44] The process is characterized by a time-dependent rate given by $k(t) = (A/\beta)(t/\beta)^{A-1}$, where A and β are the Weibull fit parameters. In the case $A > 1$ ($A < 1$), the rate of the process increases (decreases) with time, and the CCDF = $\exp(-(t/\beta)^A)$ (as illustrated by Monte Carlo simulations, Figures S6 and S7).[29] (If $A = 1$, the rate is time-independent, and the CCDF is single-exponential.) In the SMFS data, the Weibull function has been used, for example, to describe the distribution of the "on" time durations resulting from the distributed probability of radical ion pair ISC in perylenediimide single molecules dispersed in PMMA[40] and to describe heterogeneous kinetics of catalysis.[45]

The log-normal distribution has been associated with various mechanisms such as those involving several independent random variables, time-dependent rates, or stepwise processes with "memory".[46,47] The latter, for example, has been used to describe failure due to chemical reactions caused by a cumulative effect of many small multiplicative shocks, so that the rate of degradation at any given time depends on the current amount of degradation.[48] Another context for the log-normal distribution is provided by the Albery et al.[49] model that relates dispersed kinetics of various processes in heterogeneous systems to the Gaussian-distributed activation energies for such processes. In SMFS, the log-normal distribution has been utilized in, for example, describing the "off" time distribution due to distributed rates for back charge transfer[40,41] and the "on" time distribution due to those for the proton transfer.[46] In our case, it is important that both the Weibull and the log-normal distributions may suggest distributed activation energies for the processes that are responsible for the molecule's turning "on" or "off", which will be used in our discussions below.

Correlations between the Durations of the "On" Times and of the Preceding "Off" Times. Next, we examined possible correlations between the "on" time durations and the immediately preceding "off" time durations in "blinkers", which revealed interesting differences between donor-only and donor−acceptor samples (Figures 7 and S8). In particular, in donor-only samples, the duration of the following "on" times drastically decreased as the duration of the "off" time increased. In contrast, no such trend was observed in donor−acceptor samples at high acceptor concentrations (5 nm acceptor−acceptor spacing) (Figure 7), up to relatively long "off" time durations. Another way of describing these trends is that there is a considerably higher probability of obtaining long "on" time durations following a long "off" period in donor−acceptor samples as compared to donor-only samples (Figure S8). The observed drastic difference suggests that the acceptors perform a critical role during the "off" time of the F8 TCHS-Pn donor molecule by reducing the negative impact of the "off" event on the successive "on" period.

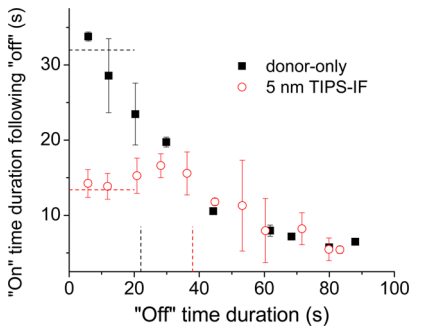

Figure 7. Correlation between an "on" time duration and the preceding "off" time duration in "blinkers" observed in donor-only and donor−acceptor samples with the 5 nm spaced TIPS-IF acceptor molecules. The lines indicate average "on" or "off" time duration (Figure 6) in the corresponding types of samples.

DISCUSSION

In this section, we discuss a physical picture consistent with our observations. To aid the description of the observed behavior, we considered a model schematically shown in Figure 8. In this model, the detected emission occurs from the excited state (2) to the ground state (1), and the transition to the state 3 corresponds to the molecule turning "off" (so that state 3 is a "dark" state). The rate responsible for this process depends on the nature of the "dark" state, which will be addressed later. Similarity of the average "on" times obtained for "blinkers" and "nonblinkers" in our samples suggests that both of these populations share the same pathway for turning "off", an observation similar to previous reports of such behavior for a variety of organic molecules incorporated in polymer matrices.[12,13] Once in the "dark" state, a "blinker" would revert back to the ground state (with a rate k_{31} that determines the "off" time duration) to be re-excited, whereas a "nonblinker" would not. Because most "nonblinkers" do not turn back "on" for at least 10 min (Figure S10), we consider these molecules "photobleached" (even if the process is reversible at longer time scales),[22] which prompts discussion of photobleaching mechanisms in acenes and in functionalized Pn derivatives in particular.

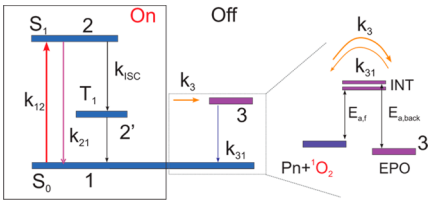

Figure 8. Model describing the processes involved and their characteristic rates. The F8 TCHS-Pn molecule is excited with a rate of k_{12} to the S_1 excited state (2) and relaxes to the ground state (1) with or without emitting a photon with a total rate k_{21}. Transitions to the triplet state T_1 occur with a rate k_{ISC}. Because of the long integration times used in our experiments, these transitions and the subsequent relaxation to the ground state occurring on the microsecond time scales are not resolved, and the molecule appears to be "on". During these cycles, there is a low probability of generating the singlet oxygen ($^1O_2$) via self-sensitization which then reacts with the F8 TCHS-Pn molecule (Pn + $^1O_2$) with a rate k_3. The reaction occurs via distributed intermediate states (INT), resulting in the formation of 6,13-TCHS-EPO (denoted as EPO). The EPO can then undergo an oxygen cleavage reaction (with a rate k_{31}) to generate the parent F8 TCHS-Pn molecule and singlet oxygen, which can react again (the case of "nonblinkers") or get re-excited (the case of "blinkers").

Photodegradation of Pn Derivatives. It has been previously shown that fluorination of the molecular core in functionalized acene derivatives considerably improved their photostability as compared to that in the nonfluorinated

DOI: 10.1021/acs.jpcc.7b03729
J. Phys. Chem. C 2017, 121, 12483−12494

derivatives.[15,50] A substantial reason for this enhanced stability is the electron-deficient nature of the fluorinated core. Addition of 8 fluorine substituents shifts the LUMO level from −3.35 eV (TIPS-Pn) to −3.6 eV (F8 TIPS-Pn), making any reaction involving electron transfer *from* the photoexcited pentacene substantially less favorable. For example, the F8 TIPS-Pn derivative incorporated in PMMA exhibits the photobleaching QY (Φ_B) a factor of ∼5 lower than that for the (non-fluorinated) TIPS-Pn derivative in PMMA.[1] An additional improvement in photostability can be achieved by a choice of bulky side groups: for example, the F8 THCS-Pn derivative under study (with bulky TCHS side groups) is about a factor of ∼2 more stable than the F8 TIPS-Pn derivative (with considerably smaller TIPS side groups) in PMMA.[15,17] As these observations were made using low concentrations of molecules dispersed in PMMA, steric inhibition of the photodimerization[51] as a possible mechanism behind this observation can be excluded. Additionally, it has been shown that oxygen plays a critical role in photobleaching of F8 R-Pn (where R represents various side groups) molecules dispersed in PMMA (Figure S11),[15] which brings into focus interactions between Pn derivatives and oxygen.

Due to the considerable importance of acenes for organic semiconductor devices, acene−oxygen interactions have been extensively discussed in the literature.[22,23,51−56] The two pathways of photo-oxidation considered for acene derivatives are via electron transfer or energy transfer to oxygen (type I and type II, respectively). The type I process results in a formation of an acene cation and superoxide (O^{2-}), whereas the type II process proceeds by the ISC followed by the energy transfer to the oxygen molecule in its ground state ($^3O_2$) that yields singlet oxygen ($^1O_2$).[23,53] Both O^{2-} and $^1O_2$ are reactive species that could attack the acene molecule leading to an endoperoxide (EPO) formation, which is the main product of acene photobleaching toward decomposition.

The relative contribution of the types I and II processes into photodegradation depends on the derivative.[22] For example, in unsubstituted Pn the dominant pathway has been identified to be a concerted type II reaction,[23] whereas for TIPS-Pn both type I and type II processes were realized, with the type I process proceeding faster. In particular, in R-Pn derivatives, triplet state energies lower than the singlet−triplet energy gap for O_2 (0.98 eV) have made the type II process inefficient.[22,52,53] However, for example, in a stable bistetracene (BT) derivative, TIPS-BT, the type II process was still dominant, even though the adiabatic triplet state energy was 0.7 eV, due to (i) a considerably higher rate of the backward electron transfer as compared to the forward one and (ii) a 0.4 eV range of possible singlet−triplet gap energies caused by energy differences in adiabatic and vertical transitions. A similar situation was reported in the unsubstituted Pn.[23] Fluorination of the Pn core has been observed to lower the triplet state energy (e.g., from 0.96 eV in the unsubstituted Pn to 0.76 eV in perfluoropentacene (PFP)).[57]

In many functionalized acenes, the EPO formation was found to be a reversible process, for example via thermolysis in an inert atmosphere, with the reversibility time scale and the activation energy for this process dependent on the derivative.[22] Of importance to our present discussion is the observation that the TIPS-EPO formed as a result of TIPS-Pn oxidation reverted to the parent TIPS-Pn molecule with a clean cleavage of the oxygen molecule. Similar observations were made on other derivatives featuring side groups with triple bonds. Therefore, the triple bonds, such as those featured by F8 TCHS-Pn molecules used in our study, protect the acene molecule from irreversible photobleaching (decomposition).[22]

As discussed earlier, the fluorinated derivatives F8 R-Pn exhibit considerably deeper LUMO energies compared with their nonfluorinated R-Pn counterparts (e.g., by ∼0.25 eV in F8 TIPS-Pn as compared to TIPS-Pn and by ∼0.9 eV as compared to the unsubstituted Pn).[17,53,58] This dramatically reduces the driving force for the type I process, making the electron transfer from the electron-deficient F8 TCHS-Pn to oxygen, with the formation of F8 TCHS-Pn cation and superoxide, highly unlikely. On the other hand, the triplet state energy for F8 TCHS-Pn is expected to be even lower than that in TIPS-Pn, and so the type II process is also inefficient. These considerations enable high photostability of F8 R-Pn derivatives. Following the arguments of ref 23 we hypothesize that the type II mechanism, in which the singlet oxygen is generated via self-sensitization and then reacts with the F8 TCHS-Pn molecule, is the dominant mechanism of photo-oxidation for this molecule. In TIPS-Pn, the types of the EPO that formed as a result of photo-oxidation were 6,13-TIPS-EPO:5,11-TIPS-EPO (98:2),[22] which suggests that our main photo-oxidation product is 6,13-TCHS-EPO. Next, we discuss experimental observations that are consistent with our hypothesis.

Nature of the "Dark" State. The reaction of an acene with a singlet oxygen toward formation of an EPO can proceed via different pathways.[22,23] For example, in the unsubstituted Pn and TIPS-BT, the concerted mechanism was found to have a lower activation energy (13.6 and 17.7 kcal/mol for Pn and TIPS-BT, respectively) for the EPO formation as compared to the stepwise mechanism.[23] On the other hand, the TIPS-Pn derivative first forms an exciplex with the singlet oxygen which then converts to the EPO.[22] Either scenario could be realized in our system, and our present experiments cannot differentiate between these relatively short-lived intermediate states (INT in Figure 8). Regardless of the nature of the intermediate state, we assign our long-lived, and potentially reversible, "dark" state (3 in Figure 8) to the 6,13-TCHS-EPO.

Photo-oxidation reactions have been previously observed using SMFS.[11,14] For example, in the case of terrylene, after the parent molecule stopped emitting (turned "off") for several seconds, the fluorescence re-emerged having a different emission rate and a spectrum that is characteristic of an EPO.[11] For some of the molecules, several photo-oxidation reactions, resulting in different reaction products, could be observed over the period of ∼60 s under photoexcitation. In the fluorescence time trajectories (such as those in Figure 3(a)), this manifests in a different count level for each "on" state following the "off" state. In our case, the dominant 6,13-TCHS-EPO product would be nonemissive ("dark") under 633 nm excitation[22] used in our experiments. When a "blinker" molecule turns back "on" following an "off" period, it signifies that the EPO reverted back to the parent F8 TCHS-Pn molecule, which then continues to emit with the same photon emission rate (Figure 3(a)) until the next cycle of singlet oxygen generation and EPO formation.

Effect of Acceptor Addition on the EPO Formation and Reversal. With an assignment of the molecule turning "off" and back "on" to the forward and reversed (backward) oxidation reactions, two pertinent questions arise regarding (i) how the observed "on" and "off" time distributions (exemplified by the CCDFs in Figure 5) are related to the kinetics of these

DOI: 10.1021/acs.jpcc.7b03729
J. Phys. Chem. C 2017, 121, 12483−12494

reactions and (ii) how the acceptor addition affects these processes. These questions are to be addressed next.

As mentioned above, both the Weibull and log-normal distributions (which provided best fits to our CCDF data) have been utilized in describing chemical reactions with a distributed activation energy. For example, in the case of Weibull distribution, the time-dependent Weibull rate $k(t)$ can be related to the activation energies via $k = k_0 \exp[-E_a/RT]$ (where k_0 is a pre-exponential factor, E_a is the activation energy, R is the universal gas constant, and T is the temperature). Then, the distribution function $D(E_a)$ for the activation energies is given by[44]

$$D(E_a) = \mathrm{PDF}(t)|dt/dE_a| = \frac{1}{RT}\frac{A}{A-1}\left(\frac{t}{\beta}\right)^{A} e^{-(t/\beta)^{A}}$$

where t is related to E_a by $E_a = -RT(\ln(A/(k_0\beta)) + (A-1)\ln(t/\beta))$ and PDF(t) is the Weibull probability distribution function $\mathrm{PDF}(t) = (A/\beta)(t/\beta)^{A-1}\exp[-(t/\beta)^{A}]$.[29] This enables extraction of the distribution functions $D(E_a)$ based on the A and β parameters obtained from fits to the "on" or "off" time durations CCDFs. In the following estimates, $k_0 = k_B T/h \approx 6.17 \times 10^{12}\ s^{-1}$ (where k_B is the Boltzmann constant, h is the Planck constant, and $T = 295$ K), used in the transition state theory, will be assumed. (This assumption determines the absolute scale for the activation energies and does not affect their distribution and/or trends discussed below.)

The average "off" time duration $\langle\tau\rangle_{off}$ is related to the rate k_{31} of Figure 8. If the "off" CCDFs were single-exponential, then k_{31} would be a constant ($\langle\tau\rangle_{off} = 1/k_{31}$), which would correspond to a single activation energy for the backward reaction $E_{a,back}$ from the EPO to the parent molecule. Because the "off" times CCDFs obtained from our data were predominantly Weibull-distributed, there is a distribution in activation energies as shown in Figure 9(b). In donor-only samples, the distribution $D(E_{a,back})$ is narrow owing to the values of the Weibull parameter A close to 1 (e.g., $A = 1.1$ for the donor-only data in Figure 9(b)). The log-normal-tending CCDFs observed in some donor-only samples (Table S2) then would indicate a more symmetric, closer to the Gaussian, distribution of activation energies. The most probable activation energy $E^0_{a,back}$ in a donor-only sample yielded a value of $E^0_{a,back} = 19.05$ kcal/mol or ~80 kJ/mol. This is lower than the ~90 kJ/mol obtained for the thermolysis reaction in several reversible functionalized acene-EPOs,[22] consistent with a more favored reverse reaction in F8 TCHS-Pn. As acceptors are added, the distribution $D(E_{a,back})$ shifts toward the higher activation energies and broadens (Figure 9(b)).

The average "on" time duration ($\langle\tau\rangle_{on}$), in a simple case of a single-exponential "on" CCDF, is related to the rate of the EPO formation (k_3 in Figure 8) by $\langle\tau\rangle_{on} = 1/(\Phi_{O2}k_3)$, where Φ_{O2} is the probability of generating singlet oxygen upon photon absorption. In our case of Weibull-distributed "on" CCDFs, the activation energies for the forward reaction ($E_{a,f}$) are distributed according to $D(E_{a,f})$ as shown in Figures 9(a) and (c), and Φ_{O2} determines the absolute scale for the activation energies given by $E^0_{a,f}$. The upper bound on Φ_{O2} is imposed by the ISC efficiency. If we assume an ISC triplet yield of ~1% (so that $\Phi_{O2} = 0.01$),[59] the most probable activation energy ($E^0_{a,f}$) in donor-only samples for "nonblinkers" yields ~16.5 kcal/mol, which is in between 13.6 and 17.7 kcal/mol obtained for concerted reactions of the unsubstituted Pn and TIPS-BT, respectively, with singlet oxygen.[23] As the F8 TCHS-Pn

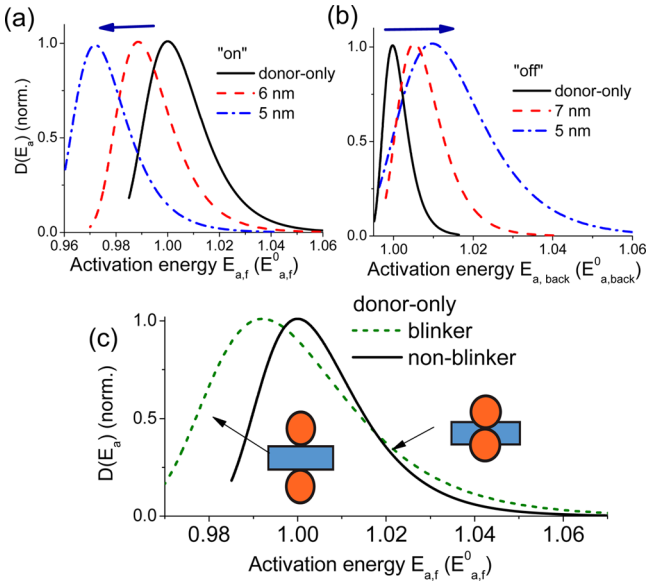

Figure 9. Distributions of activation energies for the forward ($E_{a,f}$) (a) and reversed ($E_{a,back}$) (b) reactions of the F8 TCHS-Pn with singlet oxygen. The scale is set with respect to $E^0_{a,f}$ ($E^0_{a,back}$) which is the most probable activation energy for forward (backward) reactions in donor-only samples. As the acceptors are added, the activation energies for the forward reaction shift to the lower values (a), while those for the reversed reaction shift to the higher values (b). (c) Distributions of $E_{a,f}$ for "nonblinkers" and "blinkers" in donor-only samples. The scale is set with respect to $E^0_{a,f}$ which is the most probable activation energy for forward reactions in "nonblinkers". "Blinkers" exhibit a larger population of molecules with lower activation energies as compared to "nonblinkers". The difference in the distributions is attributed to the differences in the TCHS groups conformations that make the molecule less vulnerable (right) or more vulnerable (left) for the oxygen attacks as schematically shown.

derivative is about an order of magnitude more stable[15] than TIPS-Pn, which in turn is about 50 times more stable than the unsubstituted Pn,[52] it is reasonable to expect that the activation energy for the forward reaction for F8 TCHS-Pn would be considerably higher than that for the unsubstituted Pn. However, there is an alternative scenario which yields a different scaling energy $E^0_{a,f}$ that could be operational here, as discussed below. Regardless of the absolute scale set by the value of $E^0_{a,f}$, as acceptors are added, the activation energies shift to the lower values, making the forward reaction, on average, more probable (Figure 9(a)). Figure 9(c) compares the forward reaction activation energy distributions $D(E_{a,f})$ for the "nonblinkers" and "blinkers" in donor-only samples. In spite of the similarity in their average "on" time durations (Figures 6(a) and S6), the distributions are distinctly different, with a considerably more pronounced contribution of the lower activation energies in the case of "blinkers".

One of the possibilities for the origin of the distributed activation energies in Figure 9 is in the heterogeneity of the conformations of the bulky TCHS side groups when a F8 TCHS-Pn molecule is incorporated in a PMMA matrix.[15] Some of these conformations are more protective of the molecular core with respect to reactions with oxygen (acting as an "umbrella") than others, resulting in a slightly higher or lower activation barrier for the reaction. The presence of such side-group-related effects, and protective conformations in particular, is validated by a factor of ~2 enhancement of photostability of F8 TCHS-Pn molecules as compared to F8

DOI: 10.1021/acs.jpcc.7b03729
J. Phys. Chem. C 2017, 121, 12483−12494

TIPS-Pn molecules dispersed in PMMA.[15] In this context, the difference observed in the "nonblinker" and "blinker" distributions in donor-only samples may suggest that after the oxygen cleavage during the reverse reaction the TCHS conformations are more randomized, considerably increasing the occurrence of less protected configurations. Along the same lines, the presence of acceptors reconfigures the volume available to the F8 TCHS-Pn molecule in the blend, which favors less protective TCHS conformations as compared to those in donor-only samples. This makes the photo-oxidation more probable and the reversal less probable on average.

Physical Picture. The overall physical picture consistent with observations discussed above is schematically illustrated in Figure 10. In donor-only samples, about 90% of the F8 TCHS-Pn molecules are "nonblinkers": after they turn "off" they do not turn back "on" for at least several hundreds of seconds. There are two main possibilities behind this observation: (i) as the parent molecule turns into its EPO, the activation barrier $E_{a,back}$ for the reversal is too high and (ii) the reversal does occur, but the backward reaction generates the singlet oxygen, which then attacks the molecule again before it can be re-excited. The dramatic increase in the percentage of "blinkers" as the acceptors are added (>50% in donor–acceptor samples with less than 8 nm spaced acceptors, Figure 4) indicates a considerable contribution of (ii). It also suggests that the backward reaction is a concerted process characterized by a high yield of the singlet oxygen. In donor–acceptor samples with the average acceptor–acceptor separation of <10 nm, the acceptor molecules located well within the oxygen diffusion length ($L = \sqrt{(6D\tau_{O2})} \approx 14$ nm, assuming the diffusion coefficient $D = 1.4 \times 10^{-8}$ cm^2/s and the singlet oxygen lifetime $\tau_{O2} = 25$ μs in PMMA[39,60]) from the F8 TCHS-Pn molecule, act as singlet oxygen quenchers. They protect the F8 TCHS-Pn molecule from a repeated reaction to form the EPO and enable the F8 TCHS-Pn molecule to turn "on" again, thus turning a "nonblinker" into a "blinker". The effect of the singlet oxygen quenching by acceptor molecules is also apparent from the correlations of the "on" and "off" durations of Figure 7. With the exception of rare cases of very long "off" time durations, the presence of acceptors "erases" the correlation between the "on" and the preceding "off" time duration. This suggests that the "off" event does not make the molecule more vulnerable toward further oxygen attacks (e.g., due to repeated oxidation/reversal reactions resulting in progressively less protective TCHS conformations) in donor–acceptor samples, in contrast to that in donor-only samples, as can also be appreciated from comparison of the "blinker" and "nonblinker" distributions in Figures 9(c) and S9. Even though the TCHS group conformations in F8 TCHS-Pn molecules in donor–acceptor samples are on average less protective than those in donor-only samples, making the forward reaction more probable and the reverse reaction less probable, once the reverse reaction does happen, the molecule has a considerably lower probability to immediately react again, until the next photoexcited cycle of the singlet oxygen generation, and is not more susceptible toward photo-oxidation during that cycle than before.

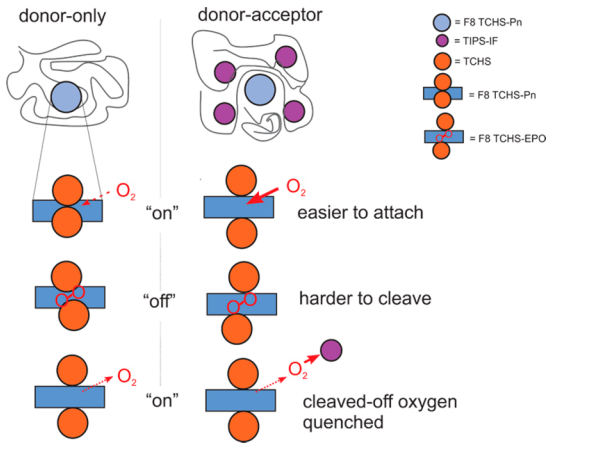

Figure 10. Schematics of the effect of acceptor-modified environment on the photophysics of F8 TCHS-Pn donor molecules. In donor-only samples, bulky TCHS side groups protect the molecule from reactions with oxygen so that the molecule can be excited up to ~10^6 times before it reacts (i.e., forms an EPO) and turns "off". Once the reaction happens, the EPO can undergo a reverse reaction to recreate the parent F8 TCHS-Pn molecule and singlet oxygen. These can react again, so that the molecule remains in the dark state ("nonblinker"), or if the reaction does not occur then the molecule is excited again and turns "on" ("blinker"). After this process, the protective conformation of the TCHS groups is partially lost so that the molecule has a higher probability to react with oxygen than it originally had. Addition of acceptors modifies the environment and resulting TCHS conformations in such a way that the activation energy for the photo-oxidation (reversal) becomes lower (higher). However, once the reverse reaction happens, the singlet oxygen is efficiently quenched by the nearby acceptor molecules, which dramatically increases the probability of the F8 TCHS-Pn molecule to be re-excited (thus, increasing the percentage of "blinkers").

The observations above invoke the following estimates. Considering for simplicity a constant value of the rate k_3 of the EPO formation and using the average "on" time $\langle\tau\rangle_{on}$, $= 1/(\Phi_{O2}k_3) = 32$ s (in donor-only samples), one obtains $\Phi_{O2}k_3 \approx 0.03$ s^{-1}. Given the photobleaching QY (Φ_B) for F8 TCHS-Pn in PMMA of ~10^{-6} and $\Phi_B = \Phi_{O2}k_3\tau_{O2}$, one obtains τ_{O2} of 32 μs (which is comparable with that of ~25 μs reported in pristine PMMA[60]). On the other hand, once the reverse reaction (EPO → parent molecule) produces singlet oxygen with a 100% yield, the probability of the repeat forward reaction is then $k_3\tau_{O2} = 0.9$, where 0.9 represents ~90% of "nonblinkers" in donor-only samples, which (assuming $\tau_{O2} = 32$ μs) yields $k_3 \approx 3 \times 10^4$ s^{-1}. This yields the probability of the singlet oxygen generation per absorbed photon, Φ_{O2}, of 10^{-6}. Such low probability would be consistent with the low adiabatic singlet–triplet energy gap making the self-sensitization a rare process. With these considerations, the most probable activation energy for the forward reaction ($E^0_{a,f}$ in Figure 9(a)) is about ~11 kcal/mol, which could correspond to that of the exciplex formation, a precursor to the EPO formation.[22,61] The addition of acceptors increases the rate k_3 due to creating morphology less protective of the F8 TCHS-Pn reactions with oxygen (resulting in a lower $\langle\tau\rangle_{on}$) but quenches the singlet oxygen as to considerably reduce the singlet oxygen lifetime τ_{O2} which dramatically reduces the probability of the immediate repeat reaction.

CONCLUSION

We obtained a molecular-level picture of the photophysics of F8 TCHS-Pn (donor) molecules in PMMA serving as a probe of evolution of the nanoenvironment due to an addition of TIPS-IF or PCBM acceptor molecules. Reversible photo-oxidation was observed, with the distributed activation energies both for the forward (parent molecule → EPO) and for the reverse (EPO → parent molecule) reactions. The acceptor

DOI: 10.1021/acs.jpcc.7b03729
J. Phys. Chem. C 2017, 121, 12483–12494

addition shifted the most probable activation energy toward the lower (higher) energies for the forward (reverse) reactions. We attribute these observations to acceptor-induced change in the polymer morphology that imposes the conformation of the TCHS side groups such that the F8 TCHS-Pn molecule is less protected from oxygen attacks. The singlet oxygen is produced in high yield in the reverse reaction but is efficiently quenched by acceptors, thus preventing the molecule from the repeat oxygen attack. Therefore, the overall photostability of the donor molecule in the presence of acceptors is determined by an interplay between the acceptor-modified morphology and the ability of acceptors to quench singlet oxygen. Understanding this interplay and how to slow down the photo-oxidation/enhance the reversibility of photo-oxidation reactions is important for improving stability of organic semiconductor devices. How this interplay is influenced by the particular features of the host polymer, electronic structure, and the side groups of the molecules will be a subject of further investigation.

■ ASSOCIATED CONTENT

Supporting Information

The Supporting Information is available free of charge on the ACS Publications website at DOI: 10.1021/acs.jpcc.7b03729.

Details of sample preparation, analysis of fluorescence time trajectories, calibration of concentrations versus intermolecular distances, FRET data and calculations, numbers of analyzed fluorophores for each sample, Monte Carlo simulations, p-values and fit parameters, "on"/"off" correlation data, distribution of activation energies, and bulk photobleaching data (PDF)

■ AUTHOR INFORMATION

Corresponding Author

*E-mail: oksana@science.oregonstate.edu.

ORCID

Michael M. Haley: 0000-0002-7027-4141

John E. Anthony: 0000-0002-8972-1888

Oksana Ostroverkhova: 0000-0002-3833-161X

Notes

The authors declare no competing financial interest.

■ ACKNOWLEDGMENTS

The authors thank A. Fox and B. Gibbons for the AFM measurements. This work was supported by the National Science Foundation (DMR-1207309 to O.O.; CHE-1565780 to M.M.H.).

■ REFERENCES

(1) Ostroverkhova, O. Organic Optoelectronic Materials: Mechanisms and Applications. *Chem. Rev.* **2016**, *116*, 13279−13412.

(2) Hunter, S.; Chen, J.; Anthopoulos, T. D. Microstructural Control of Charge Transport in Organic Blend Thin-Film Transistors. *Adv. Funct. Mater.* **2014**, *24* (38), 5969−5976.

(3) Rivnay, J.; Mannsfeld, S. C. B.; Miller, C. E.; Salleo, A.; Toney, M. F. Quantitative Determination of Organic Semiconductor Microstructure from the Molecular to Device Scale. *Chem. Rev.* **2012**, *112* (10), 5488−5519.

(4) Groves, C.; Reid, O. G.; Ginger, D. S. Heterogeneity in Polymer Solar Cells: Local Morphology and Performance in Organic Photovoltaics Studied with Scanning Probe Microscopy. *Acc. Chem. Res.* **2010**, *43* (5), 612−620.

(5) Giridharagopal, R.; Shao, G.; Groves, C.; Ginger, D. S. New SPM Techniques for Analyzing OPV Materials. *Mater. Today* **2010**, *13* (9), 50−56.

(6) Lupton, J. M. Single-Molecule Spectroscopy for Plastic Electronics: Materials Analysis from the Bottom-Up. *Adv. Mater.* **2010**, *22* (15), 1689−1721.

(7) Wilma, K.; Issac, A.; Chen, Z.; Würthner, F.; Hildner, R.; Köhler, J. Tracing Single Electrons in a Disordered Polymer Film at Room Temperature. *J. Phys. Chem. Lett.* **2016**, *7*, 1478−1483.

(8) Steiner, F.; Vogelsang, J.; Lupton, J. M. Singlet-Triplet Annihilation Limits Exciton Yield in poly(3-Hexylthiophene). *Phys. Rev. Lett.* **2014**, *112* (13), 137402.

(9) Da Como, E.; Borys, N. J.; Strohriegl, P.; Walter, M. J.; Lupton, J. M. Formation of a Defect-Free Pi-Electron System in Single Beta-Phase Polyfluorene Chains. *J. Am. Chem. Soc.* **2011**, *133* (11), 3690−3692.

(10) Diehl, F. P.; Roos, C.; Duymaz, A.; Lunkenheimer, B.; Köhn, A.; Basché, T. Emergence of Coherence through Variation of Intermolecular Distances in a Series of Molecular Dimers. *J. Phys. Chem. Lett.* **2014**, *5* (2), 262−269.

(11) Christ, T.; Kulzer, F.; Bordat, P.; Basché, T. Watching the Photo-Oxidation of a Single Aromatic Hydrocarbon Molecule. *Angew. Chem., Int. Ed.* **2001**, *40* (22), 4192−4195.

(12) Haase, M.; Hübner, C. G.; Nolde, F.; Müllen, K.; Basché, T. Photoblinking and Photobleaching of Rylene Diimide Dyes. *Phys. Chem. Chem. Phys.* **2011**, *13* (5), 1776−1785.

(13) Zondervan, R.; Kulzer, F.; Kol'chenko, M. A.; Orrit, M. Photobleaching of Rhodamine 6G in Poly(vinyl Alcohol) at the Ensemble and Single-Molecule Levels. *J. Phys. Chem. A* **2004**, *108* (10), 1657−1665.

(14) Deschenes, L. A.; Vanden Bout, D. A. Single Molecule Photobleaching: Increasing Photon Yield and Survival Time through Suppression of Two-Step Photolysis. *Chem. Phys. Lett.* **2002**, *365* (5−6), 387−395.

(15) Shepherd, W. E. B.; Grollman, R.; Robertson, A.; Paudel, K.; Hallani, R.; Loth, M. A.; Anthony, J. E.; Ostroverkhova, O. Single-Molecule Imaging of Organic Semiconductors: Toward Nanoscale Insights into Photophysics and Molecular Packing. *Chem. Phys. Lett.* **2015**, *629*, 29−35.

(16) Hallani, R. K.; Thorley, K. J.; Mei, Y.; Parkin, S. R.; Jurchescu, O. D.; Anthony, J. E. Structural and Electronic Properties of Crystalline, Isomerically Pure Anthradithiophene Derivatives. *Adv. Funct. Mater.* **2016**, *26*, 2341−2348.

(17) Kendrick, M. J.; Neunzert, A.; Payne, M. M.; Purushothaman, B.; Rose, B. D.; Anthony, J. E.; Haley, M. M.; Ostroverkhova, O. Formation of the Donor-Acceptor Charge-Transfer Exciton and Its Contribution to Charge Photogeneration and Recombination in Small-Molecule Bulk Heterojunctions. *J. Phys. Chem. C* **2012**, *116* (34), 18108−18116.

(18) Niazi, M. R.; Li, R.; Li, E. Q.; Kirmani, A. R.; Abdelsamie, M.; Wang, Q.; Pan, W.; Payne, M. M.; Anthony, J. E.; Smilgies, D.-M.; et al. Solution-Printed Organic Semiconductor Blends Exhibiting Transport Properties on Par with Single Crystals. *Nat. Commun.* **2015**, *6*, 8598.

(19) Paudel, K.; Johnson, B.; Neunzert, A.; Thieme, M.; Purushothaman, B.; Payne, M. M.; Anthony, J. E.; Ostroverkhova, O. Small-Molecule Bulk Heterojunctions: Distinguishing between Effects of Energy Offsets and Molecular Packing on Optoelectronic Properties. *J. Phys. Chem. C* **2013**, *117* (47), 24752−24760.

(20) Nasrallah, I.; Banger, K. K.; Vaynzof, Y.; Payne, M. M.; Too, P.; Jongman, J.; Anthony, J. E.; Sirringhaus, H. Effect of Ozone on the Stability of Solution-Processed Anthradithiophene-Based Organic Field-Effect Transistors. *Chem. Mater.* **2014**, *26*, 3914−3919.

(21) Di Pietro, R.; Fazzi, D.; Kehoe, T. B.; Sirringhaus, H. Spectroscopic Investigation of Oxygen- and Water-Induced Electron Trapping and Charge Transport Instabilities in N-Type Polymer Semiconductors. *J. Am. Chem. Soc.* **2012**, *134* (36), 14877−14889.

(22) Fudickar, W.; Linker, T. Why Triple Bonds Protect Acenes from Oxidation and Decomposition. *J. Am. Chem. Soc.* **2012**, *134*, 15071−15082.
(23) Thomas, S.; Ly, J.; Zhang, L.; Briseno, A. L.; Bredas, J. Improving the Stability of Organic Semiconductors: Distortion Energy versus Aromaticity in Substituted Bistetracene. *Chem. Mater.* **2016**, *28*, 8504−8512.
(24) Chase, D. T.; Rose, B. D.; McClintock, S. P.; Zakharov, L. N.; Haley, M. M. Indeno[1,2-*b*]fluorenes: Fully Conjugated Antiaromatic Analogues of Acenes. *Angew. Chem., Int. Ed.* **2011**, *50* (5), 1127−1130.
(25) Chase, D. T.; Fix, A. G.; Rose, B. D.; Weber, C. D.; Nobusue, S.; Stockwell, C. E.; Zakharov, L. N.; Lonergan, M. C.; Haley, M. M. Electron-Accepting 6,12-diethynylindeno[1,2-*b*]fluorenes: Synthesis, Crystal Structures, and Photophysical Properties. *Angew. Chem., Int. Ed.* **2011**, *50* (47), 11103−11106.
(26) Liu, T.; Troisi, A. What Makes Fullerene Acceptors Special as Electron Acceptors in Organic Solar Cells and How to Replace Them. *Adv. Mater.* **2013**, *25* (7), 1038−1041.
(27) Shepherd, W. E. B.; Platt, A. D.; Hofer, D.; Ostroverkhova, O.; Loth, M.; Anthony, J. E. Aggregate Formation and Its Effect on (opto)electronic Properties of Guest-Host Organic Semiconductors. *Appl. Phys. Lett.* **2010**, *97* (16), 163303.
(28) Shepherd, W. E. B.; Platt, A. D.; Kendrick, M. J.; Loth, M. A.; Anthony, J. E.; Ostroverkhova, O. Energy Transfer and Exciplex Formation and Their Impact on Exciton and Charge Carrier Dynamics in Organic Films. *J. Phys. Chem. Lett.* **2011**, *2* (5), 362−366.
(29) Riley, E. A.; Hess, C. M.; Whitham, P. J.; Reid, P. J. Beyond Power Laws: A New Approach for Analyzing Single Molecule Photoluminescence Intermittency. *J. Chem. Phys.* **2012**, *136* (18), 184508.
(30) Frederickson, C. F.; Rose, B. D.; Haley, M. M. Explorations of the Indenofluorenes and Expanded Quinoidal Analogues. *Acc. Chem. Res.* **2017**, *50* (4), 977−987.
(31) Paudel, K.; Johnson, B.; Thieme, M.; Haley, M. M.; Payne, M. M.; Anthony, J. E.; Ostroverkhova, O. Enhanced Charge Photogeneration Promoted by Crystallinity in Small-Molecule Donor-Acceptor Bulk Heterojunctions. *Appl. Phys. Lett.* **2014**, *105* (4), 043301.
(32) Rose, B. D.; Sumner, N. J.; Filatov, A. S.; Peters, S. J.; Zakharov, L. N.; Petrukhina, M. A.; Haley, M. M. Experimental and Computational Studies of the Neutral and Reduced States of Indeno[1,2-*b*]fluorene. *J. Am. Chem. Soc.* **2014**, *136*, 9181−9189.
(33) Chase, D. T.; Fix, A. G.; Kang, S. J.; Rose, B. D.; Weber, C. D.; Zhong, Y.; Zakharov, L. N.; Lonergan, M. C.; Nuckolls, C.; Haley, M. M. 6,12-Diarylindeno[1,2-*b*]fluorenes: Syntheses, Photophysics, and Ambipolar OFETs. *J. Am. Chem. Soc.* **2012**, *134*, 10349−10352.
(34) Rose, B. D.; Shoer, L. E.; Wasielewski, M. R.; Haley, M. M. Unusually Short Excited State Lifetimes of Indenofluorene and Fluorenofluorene Derivatives Result from a Conical Intersection. *Chem. Phys. Lett.* **2014**, *616*−*617*, 137−141.
(35) Cao, Y.; Liang, Y.; Zhang, L.; Osuna, S.; Hoyt, A. L. M.; Briseno, A. L.; Houk, K. N. Why Bistetracenes Are Much Less Reactive than Pentacenes in Diels-Alder Reactions with Fullerenes. *J. Am. Chem. Soc.* **2014**, *136* (30), 10743−10751.
(36) Willets, K. A.; Ostroverkhova, O.; He, M.; Twieg, R. J.; Moerner, W. E. Novel Fluorophores for Single-Molecule Imaging. *J. Am. Chem. Soc.* **2003**, *125* (5), 1174−1175.
(37) Lounis, B.; Deich, J.; Rosell, F. Photophysics of Ds Red, a Red Fluorescent Protein, from the Ensemble to the Single-Molecule Level. *J. Phys. Chem. B* **2001**, *105*, 5048−5054.
(38) Herz, J.; Buckup, T.; Paulus, F.; Engelhart, J. U.; Bunz, U. H. F.; Motzkus, M. Unveiling Singlet Fission Mediating States in TIPS-Pentacene and Its Aza Derivatives. *J. Phys. Chem. A* **2015**, *119*, 6602−6610.
(39) Piwoński, H.; Sokołowski, A.; Waluk, J. In Search for the Best Environment for Single Molecule Studies: Photostability of Single Terrylenediimide Molecules in Various Polymer Matrices. *J. Phys. Chem. Lett.* **2015**, *6* (13), 2477−2482.
(40) Mitsui, M.; Unno, A.; Azechi, S. Understanding Photoinduced Charge Transfer Dynamics of Single Perylenediimide Dyes in a Polymer Matrix by Bin-Time Dependence of Their Fluorescence Blinking Statistics. *J. Phys. Chem. C* **2016**, *120*, 15070−15081.
(41) Wong, N.; Ogata, A.; Wustholz, K. Dispersive Electron-Transfer Kinetics from Single Molecules on TiO2 Nanoparticle Films. *J. Phys. Chem. C* **2013**, *117*, 21075−21085.
(42) Weibull, W. A Statistical Distribution Function of Wide Applicability. *J. Appl. Mech.* **1951**, *9*, 293−297.
(43) Burnham, A. K.; Braun, R. L. *Energy Fuels* **1999**, *13* (1), 1−22.
(44) Baros, Z. Z. Weibull Cumulative Distribution Function for Modeling the Isothermal Kinetics of the Titanium-Oxo-Alkoxy Cluster Growth. *Ind. Eng. Chem. Res.* **2013**, *52*, 1836.
(45) Ng, J. D.; Upadhyay, S. P.; Marquard, A. N.; Lupo, K. M.; Hinton, D. A.; Padilla, N. A.; Bates, D. M.; Goldsmith, R. H. Single-Molecule Investigation of Initiation Dynamics of an Organometallic Catalyst. *J. Am. Chem. Soc.* **2016**, *138*, 3876−3883.
(46) Riley, E. A.; Hess, C. M.; Pioquinto, J. R. L.; Kaminsky, W.; Kahr, B.; Reid, P. J. Proton Transfer and Photoluminescence Intermittency of Single Emitters in Dyed Crystals. *J. Phys. Chem. B* **2013**, *117* (16), 4313−4324.
(47) Siano, D. The Log-Normal Distribution Function. *J. Chem. Educ.* **1972**, *49* (11), 755−757.
(48) *NIST/SEMATECH E-Handbook of Statistical Methods*, http://www.itl.nist.gov/div898/handbook/ (retrieved April 10, 2017).
(49) Albery, W. J.; Bartlett, P. N.; Wilde, C. P.; Darwent, J. R. A General Model for Dispersed Kinetics in Heterogeneous Systems. *J. Am. Chem. Soc.* **1985**, *107* (18), 1854−1858.
(50) Purushothaman, B.; Parkin, S. R.; Kendrick, M. J.; David, D.; Ward, J. W.; Yu, L.; Stingelin, N.; Jurchescu, O. D.; Ostroverkhova, O.; Anthony, J. E. Synthesis and Charge Transport Studies of Stable, Soluble Hexacenes. *Chem. Commun.* **2012**, *48*, 8261−8263.
(51) Coppo, P.; Yeates, S. G. Shining Light on a Pentacene Derivative: The Role of Photoinduced Cycloadditions. *Adv. Mater.* **2005**, *17* (24), 3001−3005.
(52) Maliakal, A.; Raghavachari, K.; Katz, H.; Chandross, E.; Siegrist, T. Photochemical Stability of Pentacene and a Substituted Pentacene in Solution and in Thin Films. *Chem. Mater.* **2004**, *16* (24), 4980−4986.
(53) Northrop, B. H.; Houk, K. N.; Maliakal, A. Photostability of Pentacene and 6, 13-Disubstituted Pentacene Derivatives: A Theoretical and Experimental Mechanistic Study. *Photochem. Photobiol. Sci.* **2008**, *7*, 1463−1468.
(54) Abu-Sen, L.; Morrison, J. J.; Horn, A. B.; Yeates, S. G. Concentration- and Solvent-Dependent Photochemical Instability of 6,13-Bis(triisopropysilylethynyl)pentacene. *Adv. Opt. Mater.* **2014**, *2* (7), 636−640.
(55) Reddy, A. R.; Bendikov, M. Diels − Alder Reaction of Acenes with Singlet and Triplet Oxygen − Theoretical Study of Two-State Reactivity. *Chem. Commun.* **2006**, 1179−1181.
(56) Fudickar, W.; Linker, T. Reversible Photooxygenation of Alkynylanthracenes: Chemical Generation of Singlet Oxygen under Very Mild Conditions. *Chem. - Eur. J.* **2011**, *17*, 13661−13664.
(57) Masubuchi, T.; Sugawara, Y.; Nakajima, A.; Masubuchi, T.; Sugawara, Y.; Nakajima, A. Adiabatic Electron Affinity of Pentacene and Perfluoropentacene Molecules Studied by Anion Photoelectron Spectroscopy: Molecular Insights into Electronic Properties. *J. Chem. Phys.* **2016**, *145*, 244306.
(58) Day, J.; Platt, A. D.; Ostroverkhova, O.; Subramanian, S.; Anthony, J. E. Organic Semiconductor Composites: Influence of Additives on the Transient Photocurrent. *Appl. Phys. Lett.* **2009**, *94* (1), 013306.
(59) Patterson, F.; Lee, H. W. H.; Wilson, W. L.; Fayer, M. D. Intersystem Crossing from Singlet States of Molecular Dimers and Monomers in Mixed Molecular Crystals: Picosecond Stimulated Photon Echo Experiments. *Chem. Phys.* **1984**, *84*, 51−60.
(60) *Singlet Oxygen: Applications in Biosciences and Nanosciences*; Nonell, S., Flors, C., Eds.; Royal Society of Chemistry; 2016; Vol. *1*, pp 459−472. DOI: 10.1039/9781782622208-00459

DOI: 10.1021/acs.jpcc.7b03729
J. Phys. Chem. C 2017, 121, 12483−12494

(61) Darmanyan, A. P.; Jenks, W. S.; Jardon, P. Charge-Transfer Quenching of Singlet Oxygen O2 (1ΔG) by Amines and Aromatic Hydrocarbons. *J. Phys. Chem. A* **1998**, *102* (98), 7420−7426.

DOI: 10.1021/acs.jpcc.7b03729
J. Phys. Chem. C 2017, 121, 12483−12494